Wavelength selection and spectral narrowing of distributed Bragg reflector quantum cascade lasers up to peak optical power

Arash Sadeghi,[1,*] Peter Q. Liu,[1,2] Xiaojun Wang,[3] Jenyu Fan,[3] Mariano Troccoli,[3] and Claire F. Gmachl[1]

[1]*Department of Electrical Engineering, Princeton University, Princeton, New Jersey 08544, USA*
[2]*Current address: Institute of Quantum Electronics, ETH Zürich, 8093, Zürich, Switzerland*
[3]*AdTech Optics, 18007 Cortney Court, City of Industry, California 91748 USA*
[*]*asadeghi@princeton.edu*

Abstract: We investigate the impact of Distributed Bragg Reflectors (DBR), ion-milled directly on top of Fabry-Perot type Quantum Cascade (QC) laser ridges, following fabrication and processing of the devices and observe a more than 10-fold reduction in spectral full-width-half-maximum (FWHM) and a maximum of 20dB side-mode suppression ratio (SMSR), maintained to peak optical power. As predicted by our model, and experimentally verified, there is a "sweet-spot" in terms of grating length, ~200 μm on a 3 mm long laser ridge, and a trade-off between spectral narrowing and output power, set by the grating depth, varied from 1.8 to 2.5 μm.

OCIS codes: (140.5965) Semiconductor lasers, quantum cascade; (140.3070) Infrared and far-infrared lasers.

References and links

1. C. Gmachl, F. Capasso, D. L. Sivco, and A. Y. Cho, "Recent progress in quantum cascade lasers and applications," Rep. Prog. Phys. **64**(11), 1533–1601 (2001).
2. Y. Yao, A. J. Hoffman, and C. Gmachl, "Mid-infrared quantum cascade lasers," Nat. Photonics **6**(7), 432–439 (2012).
3. W. W. Bewley, J. R. Lindle, C. S. Kim, I. Vurgaftman, J. R. Meyer, A. J. Evans, J. S. Yu, S. Slivken, and M. Razeghi, "Beam steering in high-power CW quantum-cascade lasers," IEEE J. Quantum Electron. **41**, 833–841 June (2005).
4. J. Faist, C. Gmachl, F. Capasso, C. Sirtori, D. L. Sivco, J. N. Baillargeon, and A. Y. Cho, "Distributed feedback quantum cascade lasers," Appl. Phys. Lett. **70**(20), 2670–2672 (1997).
5. G. Wysocki, R. F. Curl, F. K. Tittel, R. Maulini, J. M. Bulliard, and J. Faist, "Widely tunable mode-hop free external cavity quantum cascade laser for high resolution spectroscopic applications," Appl. Phys. B **81**(6), 769–777 (2005).
6. P. Q. Liu, X. Wang, J. Fan, and C. Gmachl, "Single-mode quantum cascade lasers based on a folded Fabry-Perot cavity," Appl. Phys. Lett. **98**(6), 061110 (2011).
7. L. Hvozdara, A. Lugstein, N. Finger, S. Gianordoli, W. Schrenk, K. Unterrainer, E. Bertagnolli, G. Strasser, and E. Gornik, "Quantum cascade lasers with monolithic air-semiconductor Bragg reflector," Appl. Phys. Lett. **77**(9), 1241 (2000).
8. J. Semmel, L. Nähle, S. Höfling, and A. Forchel, "Edge emitting quantum cascade microlasers on InP with deeply etched one-dimensional photonic crystals," Appl. Phys. Lett. **91**(7), 071104 (2007).
9. P. Fuchs, J. Friedl, S. Höfling, J. Koeth, A. Forchel, L. Worschech, and M. Kamp, "Single mode quantum cascade lasers with shallow-etched distributed Bragg reflector," Opt. Express **20**(4), 3890–3897 (2012).
10. A. Yariv and P. Yeh, *Optical Waves in Crystals*, (Wiley Classics Library Edition, 2003), pp. 165–176.
11. P. Q. Liu, A. J. Hoffman, M. D. Escarra, K. J. Franz, J. B. Khurgin, Y. Dikmelik, X. Wang, J.-Y. Fan, and C. F. Gmachl, "Highly power-efficient quantum cascade lasers," Nat. Photonics **4**(2), 95–98 (2010).

1. Introduction

Quantum Cascade (QC) lasers are semiconductor-based mid-infrared light sources, designed through bandgap engineering and offering promising applications due to their compact size,

#199942 - $15.00 USD Received 22 Oct 2013; revised 23 Nov 2013; accepted 29 Nov 2013; published 9 Dec 2013

range of operation and high output power [1,2]. Fabry-Perot type QC lasers, despite their high yield and cost-effective fabrication, have a relatively broadband spectral output due to the wavelength-independent reflectivity of the end facets. In addition, upon increasing the injection current, there is generally an increase of more than an order of magnitude in spectral width due to nonlinearities such as spatial and spectral hole burning in the cavity [3].

Narrowband, high power operation of QC lasers is, however, desirable in a variety of applications, such as laser-assisted surgery in medicine or countermeasures in defense. Extreme spectral narrowing to single-mode operation in QC lasers is achieved through a variety of approaches including integrating distributed feedback (DFB) gratings into the laser cavity [4], making use of an external cavity (EC) [5] or through a monolithic coupled cavity design [6]. QC lasers with deeply etched photonic band gap mirrors (PBGM) [7] and also highly reflective Distributed Bragg Reflectors (DBRs) have previously been demonstrated but did not offer an extended tuning range [8]. Another recent approach is based on introducing an electrically isolated, shallow-etched DBR section into the QC laser ridge to allow for tuning of the device over a longer spectral range [9]. Nevertheless, the above mentioned applications do not require single-mode operation, and the prevention of spectral broadening at high injection currents and optical powers is deemed sufficient, especially if it does not incur penalties on power or threshold.

2. DRB gratings design and fabrication

Here we report the fabrication and demonstration of QC lasers with a narrow band output to peak optical power, i.e. maintaining spectral broadening of less than 5 cm-1 at 4.5 μm across the entire dynamic current range, via the application of a DBR grating. In the experimental demonstration we apply the grating after the lasers are fully characterized electronically and spectrally, i.e. post-fabrication, via focused ion beam (FIB) milling.

The grating can be modeled as a multi-layer waveguide with periodically varying indices of refraction [10], the reflectivity of which depends on the number and the dimensions of the grooves, simulated via a two-dimensional finite element method (2D-FEM). The structure behaves like a distributed mirror for laser modes with frequencies lying within the resulting reflectivity stop-band, centered at the Bragg wavelength, reflecting them back into the cavity. Other frequencies will subsequently suffer a greater mirror loss at the cleaved back interface and hence have a higher lasing threshold. The grating period determines the central wavelength of the reflectivity stop-band and hence the mode selectivity of the cavity according to $\lambda_B = 2n_{eff}\Lambda_B$ where λ_B is the Bragg wavelength, n_{eff} is the effective refractive index and Λ_B is the grating period. Other parameters such as depth, profile, duty cycle and overall length of the grating also influence the coupling strength of the grating.

#199942 - $15.00 USD Received 22 Oct 2013; revised 23 Nov 2013; accepted 29 Nov 2013; published 9 Dec 2013

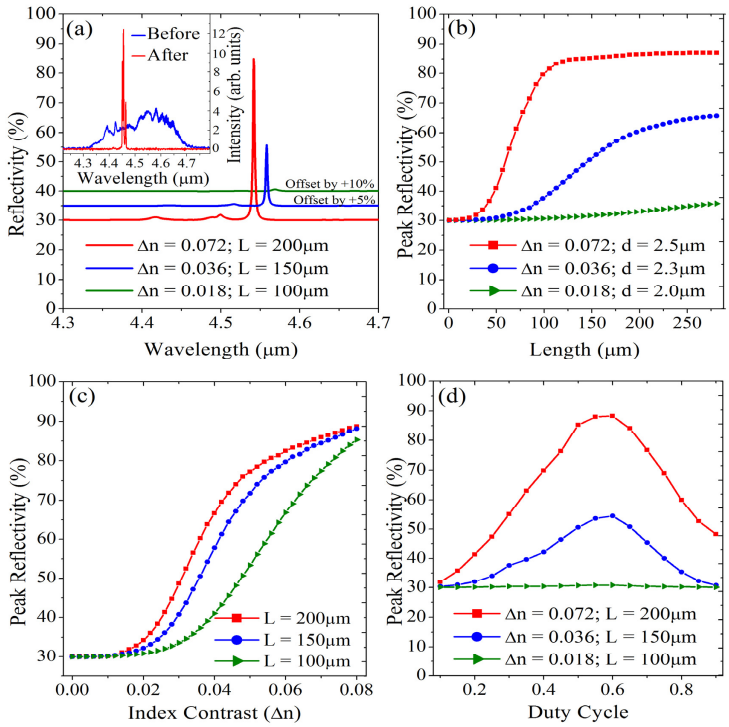

Fig. 1. Simulation of Bragg reflectivity. (a) The Bragg reflectivity as a function of wavelength is shown for gratings of length L = 200, 150, 100 μm and an index contrast of Δn = 0.072, 0.036, 0.018 respectively. The inset of part (a) shows the experimental spectral output of a laser with a 200 μm long and 2.5 μm deep (Δn = 0.072) grating. Also illustrated is the peak reflectivity as a function of (b) grating length (c) index contrast (grating depth) and (d) duty cycle.

Figure 1 shows a simulation of such a structure, where the Bragg period is chosen to be $\Lambda_B = 0.7\mu m$, corresponding to a Bragg wavelength of $\lambda_B = 4.5\mu m$ and $n_{eff} = 3.214$. Fig. 1(a) shows the simulated reflectivity of the structure, where the refractive index of the unmilled region was set to $n = 3.214$. The red, blue and green curves illustrate the reflectivity stop-band for the case of a range of grating lengths and depths. The inset of Fig. 1(a) shows the spectral output of a QC ridge laser before and after the application of a 200 μm long and 2.5 μm deep grating. The index contrast of $\Delta n = 0.02$ and 0.08 corresponds to a grating depth of 2.1 μm and 2.6 μm respectively. Figures 1(b) to 1(d) show the peak reflectivity as a function of grating length, index contrast and duty cycle. Figure 2 shows a surface plot of normalized intensity at two wavelengths, one corresponding to center wavelength of the Bragg stop-band and the other at 4 μm, demonstrating the wavelength dependent transmittance of the structure.

#199942 - $15.00 USD Received 22 Oct 2013; revised 23 Nov 2013; accepted 29 Nov 2013; published 9 Dec 2013

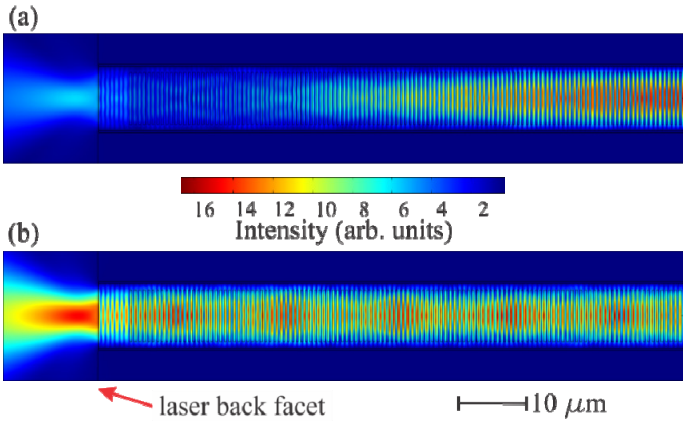

Fig. 2. Surface plot of normalized intensity where a TM polarized electric field is injected from the right and its transmission through the DBR region (285 periods) for (a) λ = 4.6 μm, corresponding to the center wavelength of the reflectivity stop-band and (b) λ = 4.0 μm, well outside of the reflectivity band. The cavity length is set to 3 mm.

According to the model, a longer grating is more favorable up to a certain length (about 200 μm or roughly 285 periods, given the parameter used for the laser), beyond which there is no advantage in extending the length. In the case of the index contrast, denoting the depth of the grating, it is found that a deeper grating would be beneficial in both maximizing the reflectivity and minimizing the spectral width of the stop-band, limited only by the thickness of the upper cladding region. The results of the simulations were later experimentally explored and found to be in good agreement.

In our approach, gratings were carved into the top cladding of the QC laser by the maskless, non-lithographic technique of Focused Ion Beam (FIB) milling. As opposed to lithographic methods, FIB milling has the main advantage of being customizable to the individual lasing characteristics of specific ridges. Figure 3 shows scanning electron microscope (SEM) images of a laser ridge following the milling process. Figure 3(b) shows a magnified view of the gratings with a cross-section cut away, illustrating the variation in the duty cycle with grating depth due to Ga + ion deposition and evaporated material re-deposition, especially in high aspect ratio features. Stitching errors and the finite resolution of the equipment also contribute to the discrepancy between the simulated and the measured values of the center wavelength of the reflectivity stop-band.

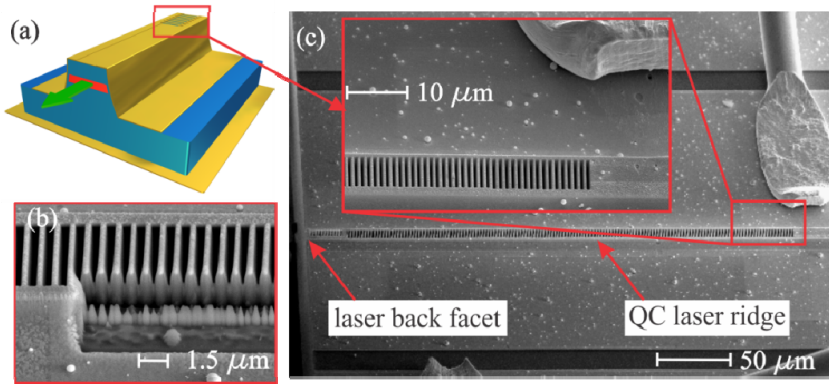

Fig. 3. (a) Schematics of a QC laser ridge with a Bragg reflector milled closer to the back facet, emphasized by the red rectangle. (b) A magnified SEM image of the grating with a cross-section cut away, illustrating the correlation between depth and duty cycle. (c) SEM images of the grating fabricated towards the back facet of a QC laser ridge.

#199942 - $15.00 USD Received 22 Oct 2013; revised 23 Nov 2013; accepted 29 Nov 2013; published 9 Dec 2013

3. DBR laser characterization

Light-current-voltage (LIV) measurements, using a fast, room temperature HgCdTe (MCT) detector, were performed before and after the application of the gratings to determine the resultant change in threshold current and peak power. The laser is mounted inside a cryostat with ZnSl windows, a collection lens, roughly 2 inches (50 mm) in diameter, is placed a focal length away; a distance of approximately 1.5 inches (38 mm). The laser ridges are all cleaved to have an overall length of 3 mm and are typically of the order of 8-25 µm in width and the grating is kept well within the ridge width. This is to avoid exposing the side-walls and hence shorting the structure and also we believe that by doing so we can reduce the number of transverse modes, hence diminish beam steering [3] well above threshold. Figure 4(a) shows the LIV characteristics of such an unstable laser, measuring 30 µm in ridge width, before and after the application of a DBR grating; the error bars denote the temporal variation of the laser's output, due to in-plane beam steering (common in wide ridge, high peak power lasers). The error bars are generated from taking multiple measurements at random time intervals. These power fluctuations were observed to be less significant when measured with a large area detector placed close to the emitting facets, suggesting that the variations are in fact due to beam pointing instabilities. Figure 4(b) shows the LIV measurements performed on a 10 µm wide ridge laser as a function of grating length (grating sections were subsequently added after repeat measurements), illustrating a small rise in threshold current density as a function of grating length and little change in optical output power collected from the front facet, away from the grating. We attribute the variations in differential resistance to experimental uncertainties associated with having to remove and repackage the device for measurement after ion milling each grating section.

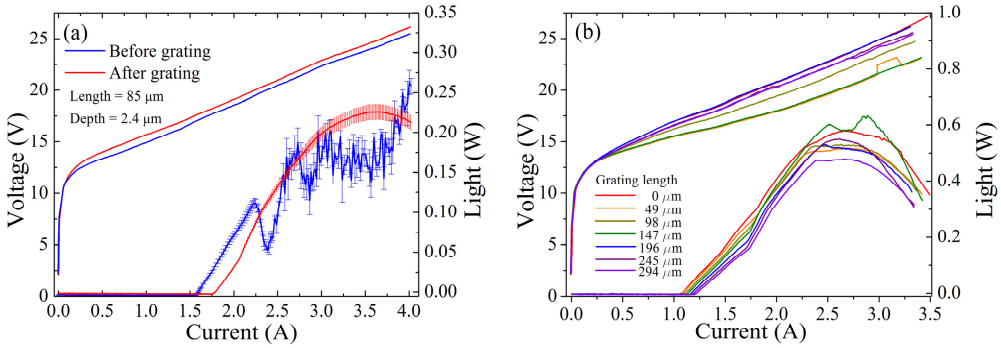

Fig. 4. (a) LIV characteristics of a 30 µm wide unstable ridge laser before and after the application of a 85 µm long, 2.4 µm deep grating. The error bars indicate the extent of the power fluctuations due to beam pointing instabilities, before the application of the grating. (b) LIV measurements from a 10 µm wide device, for grating lengths increasing from zero, in steps of 49 µm, up to 294 µm.

The laser spectra were measured at room temperature with a Fourier Transform Infrared (FTIR) spectrometer under pulsed mode operation with pulses of width 100 ns and 80 kHz repetition rate. Figure 5 shows a comparison of the spectral output measured at various current levels from threshold to the roll-over, before and after the application of the DBR. The fabricated DBR is 200 µm long and 2.5 µm deep, where the thickness of the top cladding layer is 3.4 µm (the laser structure is given in ref [11].). The results show a maximum side-mode suppression ratio of 20dB and a more than 10-fold reduction in FWHM, which was maintained to peak optical power. This latter feature is especially advantageous for the aforementioned applications and usually not a given with DFB lasers.

Also experimentally explored were the effects of changing the depth and overall length of the gratings. For length optimization, gratings of ~50 µm step size were fabricated for a range

#199942 - $15.00 USD Received 22 Oct 2013; revised 23 Nov 2013; accepted 29 Nov 2013; published 9 Dec 2013

of depths from 1.8 to 2.5 µm and the lasers were characterized at each step. As illustrated in Fig. 6(a), a maximum of 10% increase in the threshold current density was observed with increasing grating length from zero to 450 µm. We did not, however, detect a strong correlation between threshold current density and the grating depth. Figure 6(b) shows the measured peak output power as a function of grating length, showing the peak power to decrease for longer gratings. We attribute the above to a rise in scattering losses, scaling with the number of grating periods, whereas the effect is partially compensated by the expected gain from the increased reflectivity of the back facet, corresponding to the Bragg reflectivity stop-band.

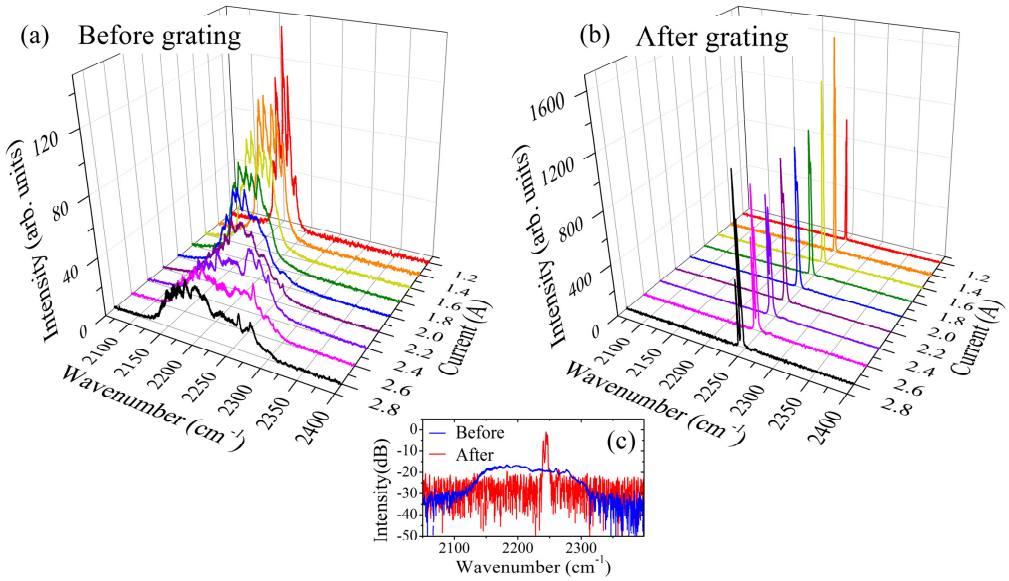

Fig. 5. The spectral output as a function of injection current covering the range from just above threshold up to and including the optical peak power (a) before and (b) after the application of the grating. The result shows a more than 10-fold reduction in FWHM and a maximum SMSR of up to 20dB, shown in (c), for a 200 µm long, 2.5 µm deep grating at peak power (I = 2.6 A).

Figure 5 shows a laser for which spectral FWHM is well defined; however, in the case of a discrete multi-peak output mode, this quantity is not well defined. Therefore, to quantify the spectral narrowing, the spectral width set by the regions in which the intensity of the modes was within 15dB of the peak intensity was measured and divided by the mode spacing, which is primarily set by the cavity length and hence an experimentally measureable constant. The result is a measure for the effective number of lasing modes. Figures 6(c) and 6(d) show this quantity plotted as a function of grating length and depth, at peak optical power for several devices. Depth measurements where performed on different lasers, given that further ion milling of an already fabricated grating in order to increase the depth proved extremely challenging experimentally. Therefor in this case the relevant metric is the difference between the number of lasing modes, before and after the application of a grating i.e. the gap between the blue and red traces in Fig. 6(d).

We conclude that, as previously predicted by our model, there is a “sweet-spot” in terms of grating length (e.g. L = 200 µm on a 3 mm laser ridge), beyond which there is little gained in spectral narrowing at the cost of a lower peak power. Furthermore, it was observed that for the device to maintain a narrowband output from threshold up to peak optical power, fabrication of a deeper grating is favorable, limited by the waveguide cladding thickness.

#199942 - $15.00 USD Received 22 Oct 2013; revised 23 Nov 2013; accepted 29 Nov 2013; published 9 Dec 2013

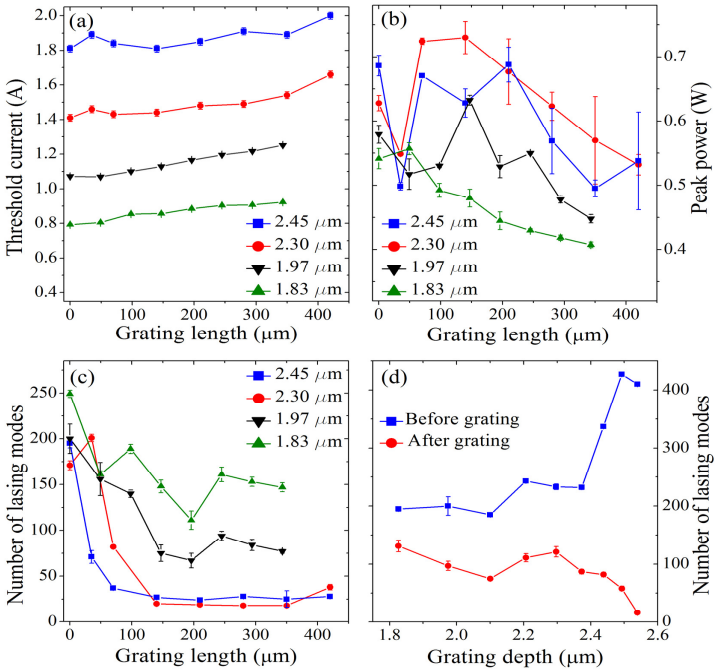

Fig. 6. The threshold current as a function of grating length for four devices (a) with gratings of different depth. (b) The laser output power as a function of grating length. (c,d) The effective number of lasing modes, quantifying the change in spectral width is shown as a function of grating length and depth at peak optical power. The grating length is set to 200 μm for the depth measurements.

4. Conclusion

In summary, we demonstrated that a DBR, on top of Fabry-Perot type QC laser ridges, leads to a more than 10-fold spectral narrowing with a maximum side-mode suppression ratio of up to 20dB, maintained to peak optical power. Our gratings were fabricated by ion-milling and experimentally exploring the grating length and depth indicated the presence of a "sweet-spot" in terms of grating length, ~200 μm on a 3 mm long laser ridge, and an apparent compromise between output power and spectral width, set by the grating depth. We also demonstrate that a deeper grating, limited by waveguide top cladding layer thickness, is required for maintaining spectral narrowing to peak optical power.

Acknowledgments

The authors would like to acknowledge imaging and analysis specialists Nan Yau and Gerald Poirier at PRISM, Princeton University. This work is supported in part by MIRTHE (NSF-ERC # EEC-0540832), NSF grant # ECCS- 1028364 and NSF grant # HRD-0833180.

#199942 - $15.00 USD Received 22 Oct 2013; revised 23 Nov 2013; accepted 29 Nov 2013; published 9 Dec 2013